Biomaterials Translational

Cellular responses to nanoscale substrate topography of TiO_2 nanotube arrays: cell morphology and adhesion

Monchupa Kingsak[1], *Panita Maturavongsadit*[1], *Hong Jiang*[2], *Qian Wang*[1,*]

Key Words:
cell adhesion; cellular responses; morphology; nanotopography; TiO_2 nanotube arrays

From the Contents

ABSTRACT

Nanotopographical features can be beneficial in augmenting cell functions and increasing osteogenic potential. However, the relationships between surface topographies and biological responses are difficult to establish due to the difficulty in controlling the surface topographical features at a low-nanometre scale. Herein, we report the fabrication of well-defined controllable titanium dioxide (TiO_2) nanotube arrays with a wide range of pore sizes, 30–175 nm in diameter, and use of the electrochemical anodization method to assess the effect of surface nanotopographies on cell morphology and adhesion. The results show that TiO_2 nanotube arrays with pore sizes of 30 and 80 nm allowed for cell spreading of bone marrow-derived mesenchymal stem cells with increased cell area coverage. Additionally, cell adhesion was significantly enhanced by controlled nanotopographies of TiO_2 nanotube arrays with 80 nm pore size. Our results demonstrate that surface modification at the nano-scale level with size tunability under controlled chemical/physical properties and culture conditions can greatly impact cell responses. These findings point to a new direction of material design for bone-tissue engineering in orthopaedic applications.

***Corresponding author:**
Qian Wang,
Wang263@mailbox.sc.edu.

http://doi.org/10.12336/biomatertransl.2022.03.006

How to cite this article:
Kingsak, M.; Maturavongsadit, P.; Jiang, H.; Wang, Q. Cellular responses to nanoscale substrate topography of TiO_2 nanotube arrays: cell morphology and adhesion. *Biomater Transl.* **2022**, *3*(3), 221-233.

Introduction

Joint arthroplasties and prosthetic implants have increased over the last few decades, likely due to the rising number of elderly people, obesity, and bone diseases.[1-3] Metals and metal alloys, including titanium, are widely used for bone replacement due to their biocompatibility, corrosion resistance, mechanical properties, and durability.[4] However, the use of metallic implants in a living body can cause some serious adverse effects, such as hypersensitivity, toxicity due to corrosion, and biofilm formation.[5, 6] Implant corrosion leads to the release of allergenic, cytotoxic, or carcinogenic species within the body causing adverse health outcomes.[7] Microbial biofilm formation on implant surface causes chronic infection, inflammation, and eventual implant failure.[8-10] Metallic implants with smooth surfaces tend to have low success rates after surgical procedures due to fibrosis and inflammatory responses that can cause osteolysis.[11] It has been shown that surface modification of metallic implants at micro-/nano-scale levels, such as increasing the surface microroughness and introducing surface nanotopography, can lessen fibrosis, promote osseointegration of metallic implants, and enhance osteogenesis of osteoblasts.[11-13] Therefore, the development of scaffolds through engineering at micro-/nano-scale levels in order to promote osteogenesis and the integration of implanted materials has been the subject of intense research.

In our early works, virus nanoparticles[14-18] and other nanoparticles[19, 20] were employed as surface coatings to create well-controlled surface nanotopographies. We found that regular topographical features at the nanometre scale promoted osteogenesis of bone marrow-derived mesenchymal stem cells (BMSCs) by upregulating the local secretion of bone morphogenetic protein-2. However, it is extremely difficult

to tune the feature size using virus-based coating materials. In comparison, titanium dioxide (TiO_2) nanotube arrays (TNAs) offer an ideal alternative as a material scaffold with controllable pore size, structural uniformity, and highly-ordered nanofeatures. TNAs can be easily synthesized through electrochemical anodization, a popular fabrication approach due to their simplicity and low cost.[21] In addition, there are many reports in the literature that TNAs can impact adhesion, migration, proliferation, and differentiation of bone cells.[22-24] We believe that cell fates, including cell differentiation, can be dictated by altering cell shapes and the cytoskeleton using underlying topography. The controllable nanotopography of TNAs under controlled culture conditions will allow us to systematically understand the effects on cellular responses, and eventually learn how to dictate cell fates using nanotopography, as well as help to further understand cell–material interactions modulated by surface topographical cues.

Focal adhesions and the cytoskeleton are linked to nanotopography-related signal-transduction events.[25] It is also believed that surface nanotopography influences either biochemical (indirect) or physical (direct) mechanotransduction, and consequently has effects on cell morphology, adhesion, proliferation, and differentiation.[25-27] Direct mechanotransduction utilizes conformational changes in the cytoskeleton to alter the shape of the nucleus and subsequently influence chromosomal arrangement and gene expression; while the indirect route utilizes biochemical messaging (i.e. G-proteins, kinases, ion channels) to convey information to the nucleus through signalling cascades.[26]

The specific alignment and dimensions of the nanoarchitecture on TiO_2 that promote cellular responses remain elusive due to discrepancies between previous reports on cell responses to different pore sizes of TNA.[28-35] Park et al.[30, 36] reported that cell adhesion, spreading, and proliferation of rat mesenchymal stem cells were the greatest on smaller diameter (15 nm) TNAs and decreased significantly with increasing pore size. Apoptosis also increased when the pore size of TNA was increased to 100 nm.[30, 36] Similarly, according to a study by Yu et al.[31] MC3T3-E1 mouse preosteoblasts exhibited greater adhesion and differentiation on 20 to 70 nm TNAs compared to 100 to 120 nm TNAs. In contrast, Oh et al.[28] demonstrated that human mesenchymal stem cells were more elongated and increased osteogenesis on larger diameter (70–100 nm) nanotubes compared to cells on 30 nm nanotubes. In addition, Zhang et al.[35] showed that primary osteoblasts adhered to 170 nm TNAs much faster and expressed higher levels of alkaline phosphatase activity compared to cells on smaller diameter (50 nm) TNAs. These contradictory results may arise from differences in cell culture conditions, cell types, and other surface properties generated during anodization, such as crystal structure, fluoride content (osteogenic element), as well as the amounts of residue on the nanotube surfaces.[22] Consequently, we aimed to establish more controllable TNAs to provide different diameter sizes but the same surface chemistries, and to see whether and how these domains of nanometre-size variations affect cell behaviours.

Methods

Formation of TiO_2 nanotube arrays for *in vitro* study

Commercially pure titanium sheets, 99.6% (Grade 2), 0.10 mm (Solution Materials, LLC, Santa Clara, CA, USA) were cut into disks with a diameter of 21 mm in order to fit into 12-well culture plates. The titanium (Ti) disks were cleaned by sonication with acetone followed by ethanol and water for 5 minutes each before anodization. Then, a Ti disk was immersed in the diethylene glycol (DEG)-based electrolyte containing 0.5 wt% ammonium fluoride (NH_4F) and 20% water and anodized at different applied voltages, 10, 20, 30, or 35 V to create TNAs with diameters of 30, 80, 120, 175 nm, respectively. After 3 hours, the anodized TNAs were sonicated in ethanol for 1 minute, immersed in deionized water, and dried under nitrogen gas. Cleaned Ti disks were used as a control group.

To evaluate the effect of differences in water content in the electrolyte on tube geometry and to determine the optimal water content for use in the electrolyte, the volume of water was varied, using contents of 1%, 5%, 10% and 20% in DEG-based electrolyte. The concentration of NH_4F at 0.5 wt%, voltage at 10 V, and anodizing time at 3 hours were controlled.

To evaluate the effect of anodization times on nanotube development, various anodizing times were used at 0, 5, 10, 15, 20, and 30 minutes. The concentration of NH_4F at 0.5 wt%, water content at 20% (v/v) in DEG-based electrolyte, and voltage at 20 V were controlled.

Characterization of anodized TiO_2 nanotube arrays

The structure of the anodized TNAs was characterized using a field emission scanning electron microscope (Zeiss Ultraplus Thermal FESEM, Carl Zeiss Microscopy GmbH, Jena, Germany). Images were captured using an in-lens detector at 5 kV. The chemical composition of the surfaces of the samples was analysed by energy-dispersive spectroscopy with scanning electron microscopy (SEM). Surface roughness was measured by atomic force microscopy (Nanoscope MultiMode & Explore SPM; Veeco, Santa Barbara, CA, USA) conducted in ambient air under tapping mode at a scan rate of 1 Hz and scan size of 10 μm × 10 μm. The larger the value, the rougher the surface.[37] To determine the surface wettability, the contact angle was calculated using the sessile drop method with a video-based contact angle system (VCA Optima, Billerica, MA, USA) at 25°C. Contact angle measurements were performed using ultrapure water as a wetting agent.

Preparation of TiO_2 nanotube array multi-well plates for *in vitro* study

After anodization for 3 hours, the synthesized TNAs were sterilized by immersion in 100% ethanol for 30 minutes then evaporated to dryness in a laminar flow hood. The sterile TNAs were then placed directly into wells of 12-well plates.

1 Department of Chemistry and Biochemistry, University of South Carolina, Columbia, SC, USA; 2 Computer Science, Physics, and Engineering Department, Benedict College, Columbia, SC, USA

Cell culture

NIH3T3 fibroblasts, and BHK-21, baby hamster kidney cells, were propagated in Dulbecco's modified Eagle's medium (Sigma-Aldrich, St. Louis, MO, USA) supplemented with 10% foetal bovine serum (FBS; Atlanta Biologicals, Flowery Branch, GA, USA), 2 mM L-glutamine, 1 mM sodium pyruvate, and 100 U/mL penicillin-streptomycin (HyClone, Logan, UT, USA) followed the literature report.[38]

BMSCs were propagated in Dulbecco's modified Eagle's medium supplemented with 10% FBS, 2 mM L-glutamine, 1 mM sodium pyruvate, 100 U/mL penicillin, 1000 U/mL streptomycin, and 0.25 μg/mL amphotericin B (MP Biomedicals, Irvine, CA, USA).

Cell cultures of NIH3T3, BHK-21, and BMSCs were incubated at 37°C in a CO_2 incubator with 5% CO_2/95% air. The medium was replaced every 3 days and the cells were trypsinized using 0.25% trypsin-ethylenediaminetetraacetic acid (Corning, Corning, NY, USA).

In vitro bone marrow-derived mesenchymal stem cell morphology study

TNA multi-well plates were prepared under sterile conditions. BMSCs at passage 7 were harvested from the tissue culture plate after reaching 80% confluence. According to the previous studies,[39, 40] BMSCs retain differentiation potentials up to passage 10. The cells were then mixed with prewarmed serum-free medium and seeded at a density of 1×10^5 cells/mL into each well, 1 mL/well, and incubated at 37°C in a CO_2 incubator with 5% CO_2/95% air. After 24 hours, the samples were washed with 1× phosphate-buffered saline (PBS; Corning) and fixed with 4% paraformaldehyde (Alfa Aesar, Tewksbury, MA, USA), pH 7.4, at 25°C, for 15 minutes. After fixation, the samples were washed several times with PBS and sequentially dehydrated in a graded series of ethanol (10%, 20%, 30%, 50%, 75%, and 100%) for 15 minutes each, and sputter-coated with a thin layer of gold (Au). SEM analyses were performed to evaluate the morphology of BMSCs grown on the surface of control Ti or different TNAs.

Confocal fluorescence microscopy

NIH3T3 cells were cultured in the prepared TNA multi-well plate at a density of 2×10^5 cells per well in serum-free medium or 10% serum-containing medium. After 24 hours of incubation at 37°C in a CO_2 incubator, the cells were stained with 5 μM Calcein AM (BioLegend, San Diego, CA, USA) for 30 min, washed several times with PBS and fixed with 4% paraformaldehyde, pH 7.4, for 15 min. The cells were further incubated with Rhodamine Phalloidin (0.1 μM; Cytoskeleton Inc., Denver, CO, USA) for 30 minutes for actin staining and Hoechst 33342 (1 μg/mL; Thermo Scientific, Waltham, MA, USA) for 5 minutes for nuclear staining. The cells were washed repetitively with PBS after each staining. The cell morphology was visualized under a fluorescence microscope (Olympus IX81, Tokyo, Japan) in disk scanning unit confocal mode.

Centrifugation assay

NIH3T3 and BHK-21 cells were harvested from tissue culture dishes after reaching 80% confluence. The cells were pre-labelled with Calcein AM (5 μM, 30 minutes) and then seeded at a density of 1.5×10^5 cells/mL into the prepared TNA multi-well plate in serum-free medium. After appropriate incubation time, TNAs and Ti disks were removed from the plate and attached to a new 12-well plate using two-sided tape. The wells then were filled to the top with serum-free medium and sealed with microplate film (Bio-Rad, Hercules, CA, USA). The plate was inverted and spun in a swinging rotor (S2096; Beckman Coulter Life Sciences, Indianapolis, IN, USA) at 25 × *g* for 5 minutes at 25°C. The old solution was carefully removed, and fresh medium was added. Afterwards, fluorescent images were taken, and ImageJ 1.53c software (National Institutes of Health, Bethesda, MD, USA) was then used to analyse the cell adhesion numbers.[41]

Image and statistical analyses

The cell adhesion numbers of NIH3T3 and BHK-21 cells, and cell areas of BMSCs were calculated from fluorescent images and SEM images, respectively, using BoneJ available in ImageJ/Fiji.[42] All cell images were converted using the same grayscale range with the purpose that all images could be compared to one another during data analysis. The percentage area coverage of BMSCs is derived from the total area of cells per total field of view area. The data are expressed as mean ± standard deviation (SD). The differences between groups were analysed by one-way analysis of variance followed by Tukey's multiple comparisons test and Student's *t*-test, using GraphPad Prism 5.0 (GraphPad Software, San Diego, CA, USA, www.graphpad.com). *P* values less than 0.05 were considered statistically significant.

Results and Discussion

Synthesis and characterization of TiO_2 nanotube arrays

To synthesize TNAs using electrochemical anodization, the Ti was placed as the anode and platinum (Pt) as the cathode in an electric circuit where a voltage was applied under magnetic stirring. The distance between the anode and the cathode was controlled at 1.5 cm. The experimental setup is shown in **Figure 1A**. The mechanism of nanotube formation is complex and occurs under interdependent conditions.[24] In simple terms, it is governed by the competition between an electrochemical etching process and a chemical dissolution process on Ti.[24, 43] Briefly, three chemical reactions occur simultaneously to create nanotube-like structures during the anodization process. The reactions are represented as follows:[44]

Water decomposition: $2H_2O \rightarrow O_2 + 4e^- + 4H^+$ (1)

Metal oxidation: $Ti + O_2 \rightarrow TiO_2$ (2)

Oxide dissolution: $TiO_2 + 6F^- + 4H^+ \rightarrow TiF_6^{2-} + 2H_2O$ (3)

The first step is field-assisted oxidation of Ti (compact oxide formation): water decomposes near the electrode and produces O^{2-} and H^+ ions. Then, the O^{2-} ions migrate to oxidize Ti. Secondly, field-assisted dissolution of TiO_2 (the initial porous structure formation) occurs: owing to the electric field, the Ti–O bond is weakened resulting in dissolution of the oxides. The final step is chemical dissolution of titanium oxides (self-organized nanotube growth): Ti^{4+} cations combine with F^- anions in the electrolyte to form a soluble hexafluorotitanium complex, resulting in fractures on the metal surface[22, 24, 43, 45, 46]

(**Figure 1B**). Due to the localized dissolution of the oxide, nanopits are formed on the TiO_2 sheet. The nanopits then convert into larger pores at higher density. Finally, the nanopores spread uniformly over the surface and become nanotubes due to the inward movement of the oxide layer at the pore bottom.[45]

In this study, we used DEG organic electrolyte containing NH_4F to prepare TNAs based on previous reports.[47, 48] The water content in the electrolyte plays a significant role in tube geometry.[23] It has been reported to increase the tube diameter and also has an impact on tube length and growth rate.[49-51] To determine the optimal water content for use in the electrolyte, the volume of water was varied, using contents of 1%, 5%, 10% and 20% in DEG-based electrolyte while controlling the concentration of NH_4F at 0.5 wt%. The result, presented in **Figure 2**, shows that after 3 hours of anodization at 10 V, none of an initial barrier TiO_2 layer was observed in the samples with higher percentages of water (10 and 20 wt%). For samples with lower percentages of water (1 and 5 wt%), the initial oxide layer remained after 3 hours of anodization. Increasing the water content from 1% to 20% led to a significant increase in electrolyte aggressiveness, which markedly reduced the time required to dissolve the native oxide at the TiO_2 surface. Based on this result, 20% water content was selected for DEG-based electrolytes in our *in vitro* study.

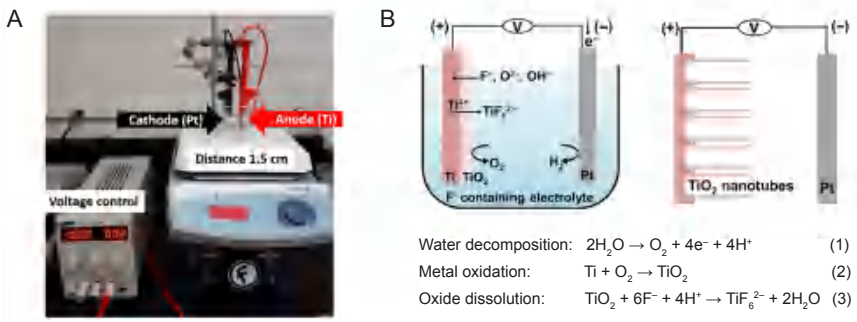

Figure 1. The synthesis of TNA by electrochemical anodization. (A) The experimental setup for the anodization of Ti. Ti was used as the anode and Pt was used as the cathode. The distance between Ti and Pt was controlled at 1.5 cm. (B) Schematic illustration showing the reactions occurring during anodization of the Ti sheet. Three chemical reactions (water decomposition, metal oxidation, and oxide dissolution) occur simultaneously to create nanotube-like structures during the anodization process. Figure 1B has been redrawn based on an original figure by Regonini et al.[44] Pt: platinum; Ti: titanium; TiO_2: titanium dioxide; TNA: TiO_2 nanotube array.

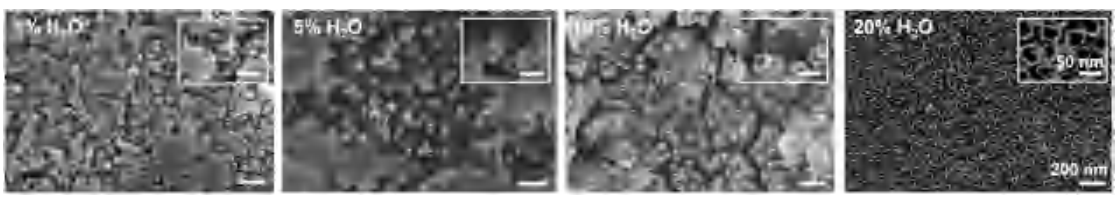

Figure 2. The effect of differences in water content in the electrolyte on tube geometry. Scanning electron microscopy images of anodized TiO_2 nanotubes prepared by anodizing Ti at 10 V for 3 hours in DEG electrolytes containing 0.5 wt% NH_4F with different concentrations of 1%, 5%, 10% and 20% (v/v) H_2O. Increasing the water content from 1% to 20% markedly reduced the time required to dissolve the native oxide during TNA formation. The insets show enlarged images of the anodized substrate prepared with different water contents in the electrolyte. All images and insets share the same scale bars at 200 nm and 50 nm, respectively. DEG: diethylene glycol; NH_4F: ammonium fluoride; Ti: titanium; TiO_2: titanium dioxide; TNA: TiO_2 nanotube array.

To observe the anodization time required for formation of the nanotube structures of TNAs, SEM images were taken of a series of samples fabricated using DEG-based electrolyte containing 0.5 wt% NH_4F and 20% water with an applied voltage of 20 V for various anodizing times. The nanotube morphology was created during the first 30 minutes of anodizing time. During the initial stage, the oxide film clearly dissolved and created continuous nanopits at 5 minutes. A nanoporous layer was generated over the surface at 10–20 minutes. With further anodization, tube-like structures were developed within 30 minutes of anodizing time (**Figure 3**). However, after 1–2 hours of anodization, some parts of the tube-like structures were shielded by a lot of residues. We found that 3 hours of anodizing time was suitable to remove most of the debris and obtain high uniformity of the nanotubes. This result also confirms that the nanotube-like structures were developed from the pits and porous structures created during removal of the surface oxide layer. The SEM image of original Ti (anodizing time at 0 minutes) was unclear due to the difficulty in adjusting the focus of camara on flat surface.

We further explored the potential range for generating a series of TNAs with controllable diameters. It has been shown by a number of reports that the diameter of nanotubes varied mostly with the applied voltage.[47, 52, 53] SEM images (**Figure 4A**, and **B**) show tube morphologies and tube lengths when

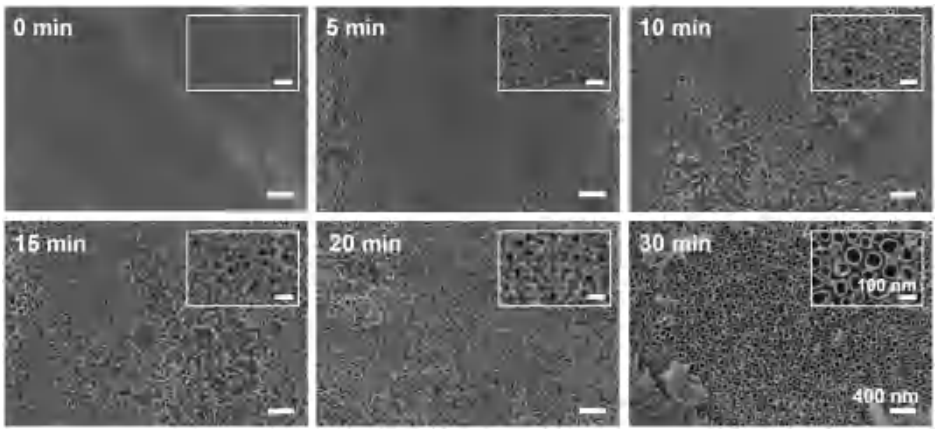

Figure 3. The effect of anodization times on nanotube development and structure. Scanning electron microscopy images show the evolution of nanotube formation during different anodizing times at 20 V for 5, 10, 15, 20, or 30 minutes in DEG-based electrolyte containing 0.5 wt% NH_4F and 20% (v/v) H_2O. Nanopits were created at 5 minutes, nanoporous layer was generated over the surface at 10–20 minutes, and nanotubes were developed at 30 minutes of anodizing times. The insets show enlarged images of the anodized substrate at different anodizing times. All images and insets share the same scale bars at 400 nm and 100 nm, respectively. DEG: diethylene glycol; NH_4F: ammonium fluoride.

applied voltages varied from 10 V to 35 V, anodized for 3 hours in DEG-based electrolyte containing 0.5 wt% NH_4F and 20% (v/v) water. No barrier TiO_2 residues remained on the anodized TNAs, and the tubular structures were smooth and consistent in every repeat. Nevertheless, as shown in **Table 1**, the higher the applied voltage, the wider the range of diameters with higher variation, which may be caused by the formation of a discontinuous nanotubular layer at high voltages, and more evident spacing between tubes.[47] The average diameters of TNAs at 10, 20, 30 and 35 V anodization, were 30, 80, 120 and 175 nm, respectively. Similarly, the average lengths of TNAs were 0.6, 1, 1.7, and 2.3 μm, respectively (shown in **Table 1**) although it was previously shown that nanotube length had no significant impact on cell function.[54] In other words, raising the applied voltage increased both nanotube diameter and length. However, when applying a high potential at 50 V for 3 hours, a sponge-like structure was observed (data not shown), similar to previous reports.[51, 55] The prepared TNA substrates in this study were designated according to their average diameter as TNA30, TNA80, TNA120, and TNA175, synthesized with applied voltages at 10, 20, 30, and 35 V, respectively.

Table 1. The chemical components, diameters and lengths of the anodised TNAs using 0.5% NH_4F with 20% (v/v) H_2O in DEG-based electrolyte under different voltages

	Ti	TNA30 (10 V)	TNA80 (20 V)	TNA120 (30 V)	TNA175 (35 V)
Element (weight%)					
O	–	23.75	23.09	22.48	22.74
F	–	6.57	6.47	6.28	6.31
Ti	100	69.68	70.44	71.24	70.96
Diameter (nm)	–	31.1±5.0	78.3±16.8	120.9±27.5	174.2±31.4
Length (μm)	–	0.6±0.1	1.0±0.1	1.7±0.1	2.3±0.4

Note: The values represent the weight% of each element, and the mean ± SD of the diameter and length (n = 3). DEG: diethylene glycol; F: fluorine; NH_4F: ammonium fluoride; O: oxygen; Ti; titanium; TNA: titanium dioxide nanotube array.

Surface wettability is well known as a key factor, which governs cellular responses. The lower the contact angle, the more hydrophilic the surface. A surface is characterized as hydrophilic when the water contact angle is < 90°, and hydrophobic when the contact angle is > 90°.[56, 57] **Figure 4C** shows the data obtained from contact angle measurements. The generated TNAs were more hydrophilic than Ti. Specifically, the surface of Ti metal alone exhibited a contact angle of 60°, while TNA30, TNA80, TNA120, and TNA175 had contact angles of 17°, 16°, 9°, and 7°, respectively. It was previously shown that the hydrophilicity of the samples increased following anodization voltage due to higher surface areas generated by increases in the diameter, spacing, and length of the nanotubes, as well as the thicker oxide suface.[58]

Energy dispersive spectroscopy revealed the chemical components of TNAs prepared under the selected preparation conditions using DEG-based electrolyte. As shown in **Table 1**, the mass fraction of titanium was approximately 70%, while oxygen made up approximately 30% of every sample. The mass fraction of fluoride was also observed in all samples at similar amounts, approximately 6%, which is commonly found due to the electrochemical anodization reaction. Control of the chemical composition, especially the fluoride content, on the TNA surfaces is important for *in vitro* cell study due to its impact on cell behaviours. Specifically, fluoride ions are known to promote osteogenic differentiation and biomineralization.[50, 59, 60] The results confirm that the chemical compositions of anodized TNA were controlled.

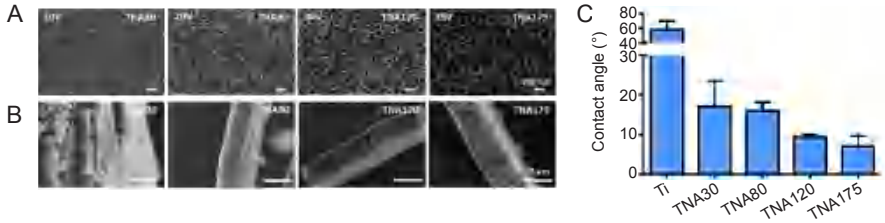

Figure 4. Characterization of sample nanostructure and surface wetting. (A, B) Top-view (A) and side-view (B) scanning electron microscopy images of TNAs prepared by anodizing Ti in DEG-based electrolyte containing 0.5 wt% NH_4F and 20% (v/v) H_2O at 10, 20, 30, and 35 V for 3 hours. The tube diameter and length were increased respectively by raising the applied voltage of anodization. Scale bars: 200 nm in A and 2 μm in B. (C) Surface wettability of TNAs at different diameters of pore size (30, 80, 120, and 175 nm). Data are expressed as mean ± SD (n = 6). DEG: diethylene glycol; NH_4F: ammonium fluoride; Ti; titanium; TNA: titanium dioxide nanotube array.

It has been reported that cell behaviours including cell adhesion, migration, proliferation, and differentiation are correlated to surface roughness.[61, 62] To investigate the surface roughness, atomic force microscopy was performed in this study. The root mean square roughness of TNA30, TNA80, TNA120, and TNA175, was approximately 94, 92, 92, and 97 nm, respectively, with no statistically significant difference (**Figure 5**). The root mean square roughness of Ti starting material was approximately 5 nm (data not shown). This implies that the influence of surface roughness of TNAs on cell behaviours was controlled.

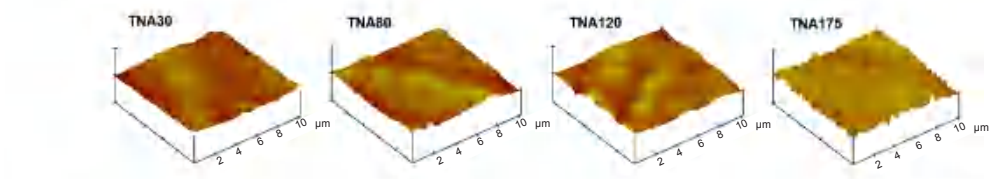

Roughness	TNA30	TNA80	TNA120	TNA175
RMS (nm)	93.7 ± 19.1	91.8 ± 19.4	92.4 ± 26.3	97.0 ± 2.2
RA (nm)	72.7 ± 14.1	68.1 ± 22.2	71.4 ± 20.9	76.6 ± 1.9

Figure 5. Summary of the surface roughness of TNAs with different diameters (30, 80, 120, 175 nm). The roughness was characterized by atomic force microscopy. The data are expressed as mean ± SD (n = 4). No significant change was observed in any comparisons based on one-way analysis of variance followed by Tukey's multiple comparisons test. Ra: mean roughness; RMS: root mean square roughness; TNA: titanium dioxide nanotube array.

Cell studies on two-dimensional cell cultured-TiO_2 nanotube array plates

Morphology of bone marrow-derived mesenchymal stem cells cultured on TiO_2 nanotube arrays

To investigate cell morphology in response to four different diameters of TNA substrates or Ti as a control, BMSCs were seeded onto the substrates and incubated for 24 hours in serum-free medium. We found that BMSCs cultured on TNA30 and TNA80 exhibited good spreading all over the surface, with a more flattened morphology compared to those on the other TNAs or Ti. Additionally, lamellipodia and filopodia were more clearly observed on the cells cultured on TNA80 compared with those on other substrates. Meanwhile, the cells cultured on TNA120 and TNA175 lost their planar shape and adopted a rounded shape with poor spreading, while few protrusions were observed, especially on TNA175, as shown in **Figure 6A**. The data in **Figure 6B** reveals that cells cultured on TNA80 showed the highest area coverage at 27%, which was significantly higher than those on TNA120 or TNA175 with area coverage at 18% and 16%, respectively. Additionally, the area coverage of the cells cultured on TNA30 (25%) was significantly higher than that on TNA175. In summary, BMSCs cultured on TNA30 or TNA80 showed an increase in cell spreading and increased percentage cell area coverage compared to the other substrates tested.

Morphology of NIH3T3 cells cultured on TiO_2 nanotube arrays

The morphology of NIH3T3 cells cultured on TNA substrates was visualised using confocal fluorescence microscopy. FBS is a growth supplement used in cell culture medium. It provides vitamins and essential compounds including binding and attachment factors required for cell attachment, growth, and proliferation.[63, 64] However, seasonal and geographical batch-to-batch variations and undefined compositions of FBS have been shown to affect cell morphology, proliferation, and differentiation in *in vitro* studies.[63, 65, 66] Serum components have not been standardized due to the complexity of their composition.[67] In this study, we observed the cell morphology of NIH3T3 cells cultured on TNA substrates with and without the addition of FBS. The confocal laser scanning microscopy result shown in **Figure 7** demonstrates that the morphology of NIH3T3 cells cultured in serum-containing medium showed good spreading of the polygonal stellate cells with elongated protrusions and more actin filaments linking to adjacent cells. On the other hand, the cells cultured in serum-free medium showed poor spreading and displayed spindle-shaped or

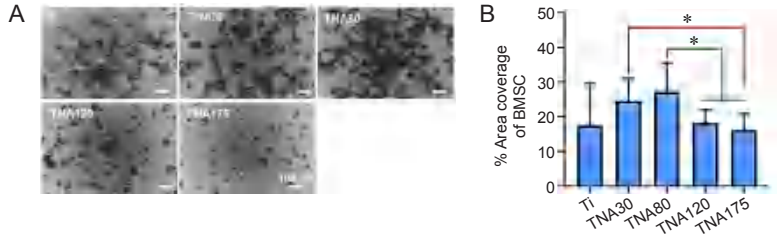

Figure 6. Morphology of BMSCs cultured on Ti or TNA substrates in two-dimensional cell culture without foetal bovine serum. TNA30 and TNA80 enhanced cell spreading and percentage cell area coverage of BMSCs. (A) SEM images show the morphology of BMSCs cultured on Ti or TNA substrates prepared by anodizing Ti in a DEG-based electrolyte at 10, 20, 30, or 35 V for 3 hours. The cells cultured on TNA30 and TNA80 exhibited good spreading all over the surface, while cells on TNA120 and TNA175 adopted a rounded shape with poor spreading. All scale bars share a length of 100 μm. (B) Percentage area coverage of BMSCs on Ti or TNA substrates, calculated from SEM images using ImageJ. Data are expressed as mean ± SD (n = 3). *P < 0.05 (Student's t-test or one-way analysis of variance followed by Tukey's multiple comparisons test). BMSC: bone marrow-derived mesenchymal stem cell; DEG: diethylene glycol; SEM: scanning electron microscopy; Ti; titanium; TNA: titanium dioxide nanotube array.

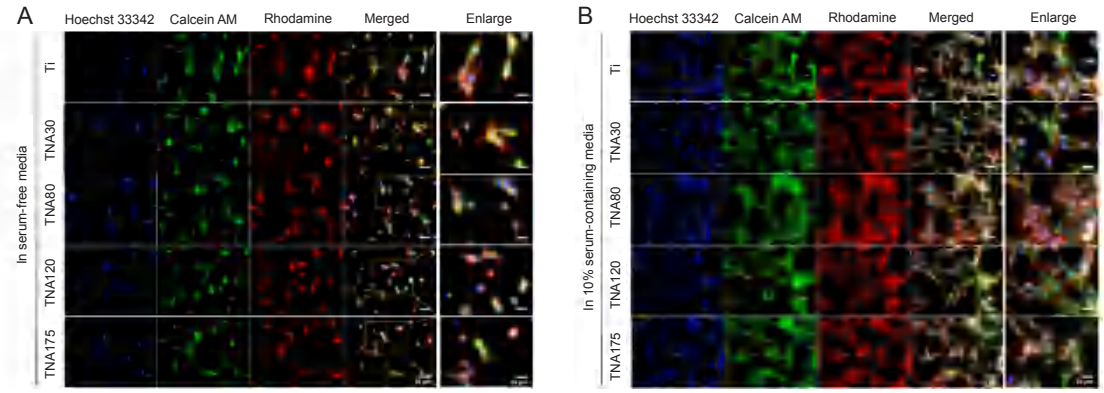

Figure 7. Morphology of NIH3T3 cells cultured on Ti or TNA substrates in two-dimensional cell culture with and without FBS. FBS significantly affected cell morphology and proliferation. (A, B) Confocal laser scanning microscopy images of NIH3T3 cells cultured on Ti or TNA substrates after 1 day of incubation in serum-free medium (A), and in 10% serum-containing medium (B). The morphology of NIH3T3 cells cultured in serum-containing medium showed good spreading, while the cells cultured in serum-free medium showed poor spreading and fewer cells. Cells were fixed and stained with Hoechst 33342 (blue fluorescence), Calcein AM (green fluorescence), and Rhodamine phalloidin (red fluorescence). The scale bars indicate a length of 50 μm for all images and 25 μm for the enlarged images. FBS: foetal bovine serum; Ti; titanium; TNA: titanium dioxide nanotube array.

spherical morphology with fewer cells and reduced actin filaments. However, there was no obvious difference in cell morphology among the control Ti and TNA samples either in serum-containing or serum-free medium when visualised under the microscope. In order to profile non-apparent morphological differences in the cells on each of the substrates, machine learning-based data processing could be used in future analysis of cell images.

Centrifugation assay to assess the cell adhesion of NIH3T3 and BHK-21 cells on TiO_2 nanotube arrays

Cell adhesion is essential for the early osseointegration of bone cells into implanted biomaterials because it is involved in stimulating intracellular signalling networks that regulate cellular behaviours and functions.[68, 69] Cell-substrate interactions are an important consideration in biomaterial development, and the most straightforward way to evaluate them is a centrifugation assay.[68, 70] As mentioned in previous sections regarding the impacts of surface wettability and roughness of the substrates on cell behaviours, nanotopographic features of the substrates also play an important role in cell adhesion. To determine the adhesive properties of NIH3T3 and BHK-21 cells cultured on Ti and TNA substrates, the centrifugation cell adhesion assay was performed. These two cell lines were selected in the assay followed the previous study.[38] The rationale is that NIH3T3 cells secrete extracellular matrix (ECM), which provides structural support for cell adhesion and migration. BHK-21 cells, unlike NIH3T3, produce much lower levels of ECM proteins.[38, 71] This allows us to observe cell attachment on substrates with and without the influence of ECM proteins secreted by cells. In addition, BMSCs were not chosen to perform in this assay because of their uncertainty in molecular and cellular changes occurred during aging of stem cells.[72-74] In other words, different passaging number of BMSCs alters cell characteristics due to their ability to undergo differentiation and may affect cell adhesion results in the centrifugation assay. Furthermore, to prevent serum proteins from adsorbing onto the substrate surface and promoting cell attachment, serum-free medium was used in this study.

The fluorescent images of NIH3T3 cells (**Figure 8A**), and BHK-21 cells (**Figure 8B**), cultured on TNAs, Ti, and tissue culture plate (polystyrene) were taken before and after spinning down in the centrifugation assay. As shown by the centrifugation assay results (**Figure 8C**), a significantly higher percentage of the NIH3T3 cells remained on the TNA80, at 66%, compared with TNA120 (44%) and TNA175 (31%) after the cells were incubated with the substrate for 1 hour. At later time-points (2 and 8 hours), the percentage of the NIH3T3 cells remaining on all TNA substrates however showed no significant difference. Additionally, BHK-21 cells cultured on TNAs showed similar trends in the numbers of remaining cells. The percentage of remaining BHK-21 cells on TNA80 (51%) was significantly higher than those on TNA120 (28%) or TNA175 (28%) after incubation for 2 hours, as shown in **Figure 8D**. However, no significant difference was observed between the different TNA substrates when incubated with BHK-21 cells for 1 or 8 hours. At 8 hours of incubation time, the cell attachment of both cell lines decreased because the deprivation of serum from the medium can reduce cell survival and increase apoptosis.[75] In summary, TNA80 promoted cell-substrate interaction and showed enhancement of cell adhesion in the early stage of cell attachment when compared with other TNAs or Ti in the centrifugation cell adhesion assay. One possible reason could be that the pore size of 80 nm might have an impact on integrin assembly and focal adhesion sites which could lead to tighter attachment compared with other pore sizes. Normally, integrin-mediated adhesions involve the binding of integrin with its ligands in ECM and the linkage to actin cytoskeleton through anchor proteins, including talin, α-actinin, and filamin, and linker proteins such as talin and vinculin.[76, 77] The clustering of the integrins and the formation of focal adhesions are then occurred and further activate intracellular signalling pathways and thereby regulate cellular responses.[78] The principal process of integrin assembly and focal adhesion formation should be similar among the different cell types. TNAs with a wide range of pore sizes were designed to mimic the native ECM nanostructures. Therefore, this adhesion result may contribute to other cell types.

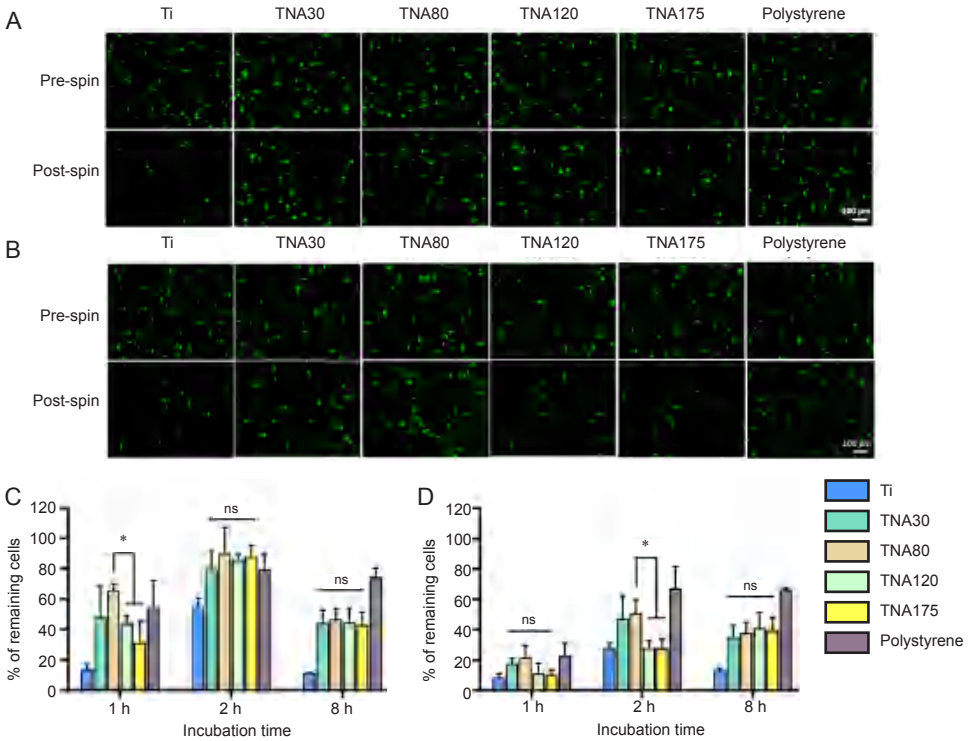

Figure 8. Assessment of the adhesion of NIH3T3 and BHK-21 cells by centrifugation assay. TNA80 promoted enhanced cell adhesion in the early stage of cell attachment. (A, B) Fluorescent images show NIH3T3 cells (A) and BHK-21 cells (B) attached on Ti, TNAs, and tissue culture plate (polystyrene) and incubated in serum-free medium for 1 and 2 hours, respectively, before and after spinning. After post spin, NIH3T3 and BHK-21 cells cultured on TNA80 detached from the substrate fewer than those on TNA120 and TNA175 after 1 and 2 hours of incubation time, respectively. The cells were stained with Calcein AM. The scale bar indicates a length of 100 μm. (C, D) The percentage of remaining NIH3T3 cells (C) and BHK-21 cells (D) after centrifugation following different incubation times. Data are expressed as mean ± SD ($n = 3$). *$P < 0.05$ (Student's t-test and one-way analysis of variance followed by Tukey's multiple comparisons test). ns: not significant; Ti; titanium; TNA: titanium dioxide nanotube array.

Conclusions and Perspectives

The success of implants greatly depends on the initial interactions between bone tissue and the implant which can be modulated by surface topography of the scaffolding materials.[79] The surface topography and nanoarchitecture strongly influence cellular behaviours, and cells recognize variability in topographic and environmental cues.[14, 79-81] However, so far, the details of the underlying mechanisms

by which nanotopographical cues regulate cellular responses remain unclear. In various studies, scaffolds with different surface topographies and properties have been developed to mimic the natural ECM environment for bone tissue.[16, 82, 83] In our previous reports, we employed plant viruses as building blocks to create nanotopographical features to study osteogenic differentiation of BMSCs. We found that coating substrates with turnip yellow mosaic virus, a spherical plant virus, and tobacco mosaic virus as the prototypical nanorods promoted early mineralization, up-regulation of osteospecific genes, and osteogenic differentiation of BMSCs to osteoblasts when compared with a flat surface.[14, 15] Furthermore, substrates coated with tobacco mosaic virus chemically modified with phosphate moieties further enhanced the expression of osteospecific genes compared with unmodified tobacco mosaic virus-coated substrates or flat Ti.[16] This suggested that the cells can sense nanotopography and surface chemistry of an underlying substrate resulting in a difference in gene expression profiles and cell behaviours.

In the orthopaedic field, more than 95% of orthopaedic implants are metallic implants because of the favourable properties of durability and fracture toughness of metals.[84] Titanium is one of the most important materials used for implantation in orthopaedic surgery because of its high strength, rigidity, great corrosion resistance, biocompatibility, similar mechanical properties to bone, and paramagnetic properties meaning that it is weakly magnetized by magnetic resonance imaging.[84-87] However, implant failure commonly occurs due to the lack of osseointegration with the smooth surface of titanium leading to increased costs and complications for patients.[11, 16, 86] Aseptic loosening of implants is a major cause of failure which contributes to 60–70% of cases for revision surgery.[86] In order to improve osseointegration, extensive efforts have largely focused on increasing the surface roughness of materials and introducing surface nanotopography. Although the mechanisms driving cellular responses guided by topographical cues are not fully known, one possible explanation is that integrins transduce extracellular forces altered by topography into biochemical signals through focal adhesions.[81, 88] Topography alters cellular responses by utilizing conformational changes in the cell cytoskeleton and effectively enhances ECM synthesis by adherent cells.[26, 88]

The nanoscale modification of a material surface to mimic the cellular environment, the ECM, could favour rapid bone accrual and effect cell interactions.[88] A great variety of techniques have been used to generate nanoscale topographic features and surface roughness on Ti implant surfaces as shown in **Table 2**.[88-91] One of the evolutional techniques of surface morphological control is the formation of TNAs by electrochemical anodization which is considered to be a more controlled, simple, and low-cost process compared to other treatments.[92] The materials that can be used with this method are titanium, aluminium, zirconium, magnesium, niobium, tantalum, tungsten, and metal alloys.[93-95] In order to produce highly ordered nanotube arrays, electrochemical anodization and lithography method can be used. The disadvantage of anodization method is that all parameters using in the synthetic process such as voltages, water content, electrolyte, etc., affect tube geometry and must be optimized in order to get the wanted nanometre-size of the pore. To compare with lithography method, it may introduce embedded ionic impurities during the anodization process and may have defects.[96, 97] However, the main disadvantages of lithography are the high cost of manufacturing and the limited working area.[97] The ability to control the properties of TNAs, especially pore diameter, by controlling the synthetic conditions of anodization allowed for the optimization of the Ti surface.[98, 99] TNAs exhibit isotropic topography arranged in an organized manner with structural uniformity in all directions.[81, 88] The controllable nanotopography of TNAs with highly ordered and controllable pore sizes is one of the key features that allow us to better understand cellular changes in response to surface topographical cues and the ways in which cells perceive variations of surface topography at the nanometre-size range.

Table 2. Various techniques used to generate nanotopographical features and surface roughness on implant materials

Physical techniques	Chemical techniques	Coating techniques	Others
Grit blasting	Anodization	Sol-Gel coating	Lithography
Nanoparticle compaction	Acid treatment	Self-assembly of monolayers	Ultraviolet photofunctionalization
	Alkali treatment	Discrete crystalline deposition	
	Hydrogen peroxide treatment	Plasma spray	
	Chemical vapor deposition	Ion implantation	
		Sputtering	
		Pulsed laser deposition	
		Electron beam evaporation	

The development of nanotopographical features on substrates can lead to improved cell-substrate interactions and provide for the creation of improved implant surfaces.[100] Although the impacts of pore size of nanotube-modified substrates on cell behaviours have been extensively studied, as reported in the literatures,[28, 30-35, 100, 101] the effect of specific diameters of TNAs on promotion of cellular responses remains inconclusive. This study provides the first comprehensive assessment of cell adhesion on well-defined and controllable TNAs with a wide range of pore sizes. A study of the cell morphology of BMSCs indicates that TNAs with smaller pore sizes, TNA30 and TNA80, provided better cell spreading and significantly greater cell area coverage compared to other TNAs with larger pore sizes. We also found that the addition of FBS to cell culture medium has an impact on cell morphology and spreading in NIH3T3 cells. To eliminate possible factors affecting cell

adhesion, we used serum-free medium in the centrifugation cell adhesion assay and performed a time-course study with different incubation times at 1, 2 and 8 hours. The results demonstrate that the highest remaining percentages of both NIH3T3 and BHK-21 cells were present after incubation of the cells on the TNA80 substrate at 1 and 2 hours, respectively. Thus, this research provides evidence that cell adhesion can be significantly enhanced using controlled nanotopographies, and an 80-nm pore size of TNA showed a promising effect on cell adhesion. In future studies, assessment of focal adhesion, protein, and gene expression could be performed to evaluate the mechanisms involved in cellular responses altered by nanometre-size topographical features. Additionally, the osteogenesis study of BMSCs could be performed to evaluate the effect on different pore sizes. The limitation of this study was that the crystallinity of TNAs was not controlled and characterized due to the limitation of the X-ray diffraction instrument in our resources.

In summary, controllable nanostructured surfaces created by anodization of Ti were established to study the optimal control of cell physiology. We believe that by changing the dimensions of the Ti nanofeatures, a highly active Ti surface can be developed to provide a solid and practical foundation of effective substrates for advanced biomaterials and orthopaedic implant designs.

Author contributions

Conceptualization, methodology, project administration and funding acquisition: HJ, QW; study design and data generation: MK, PM; data collection, investigation, and validation: MK, PM, and QW; manuscript review and editing: MK, PM, HJ, QW. All authors approved the final version of this manuscript.

Financial support

The authors gratefully acknowledge financial support from the National Science Foundation and SC EPSCoR IDeA program under NSF Award #OIA 1655740 and GEAR CRP Award Number 18-GC01.

Acknowledgement

We wish to acknowledge the work of an undergraduate student, Ayse Turhan-Comert, for applying artificial intelligence technology to explore the differences in cell activity on Titanium-based substrates. She is a student at Benedict College, a Historically Black Colleges and Universities, under guidance of Dr. Hong Jiang. Her efforts provided some preliminary ideas for this research.

Conflicts of interest statement

The authors declare no conflict of interest.

Editor note: Qian Wang is an Editorial Board member of *Biomaterials Translational*. He was blinded from reviewing or making decisions on the manuscript. The article was subject to the journal's standard procedures, with peer review handled independently of this Editorial Board member and his research group.

1. Gibon, E.; Amanatullah, D. F.; Loi, F.; Pajarinen, J.; Nabeshima, A.; Yao, Z.; Hamadouche, M.; Goodman, S. B. The biological response to orthopaedic implants for joint replacement: Part I: Metals. *J Biomed Mater Res B Appl Biomater.* **2017**, *105*, 2162-2173.
2. Cherubino, P.; Ratti, C.; Fagetti, A.; Binda, T. Total hip arthroplasty and bone fragility. *Aging Clin Exp Res.* **2011**, *23*, 76-77.
3. Etkin, C. D.; Springer, B. D. The American Joint Replacement Registry-the first 5 years. *Arthroplast Today.* **2017**, *3*, 67-69.
4. Saini, M.; Singh, Y.; Arora, P.; Arora, V.; Jain, K. Implant biomaterials: a comprehensive review. *World J Clin Cases.* **2015**, *3*, 52-57.
5. Guo, X.; Wang, Q. Magnesium-based biodegradable metal materials: past, present and future. *Biomater Transl.* **2021**, *2*, 175-176.
6. Jing, X.; Ding, Q.; Wu, Q.; Su, W.; Yu, K.; Su, Y.; Ye, B.; Gao, Q.; Sun, T.; Guo, X. Magnesium-based materials in orthopaedics: material properties and animal models. *Biomater Transl.* **2021**, *2*, 197-213.
7. Eliaz, N. Corrosion of metallic biomaterials: a review. *Materials (Basel).* **2019**, *12*, 407.
8. Shokeen, B.; Zamani, L.; Zadmehr, S.; Pouraghaie, S.; Ozawa, R.; Yilmaz, B.; Lilak, S.; Sharma, S.; Ogawa, T.; Moshaverinia, A.; Lux, R. Surface characterization and assessment of biofilm formation on two titanium-based implant coating materials. *Front Dent Med.* **2021**, *2*, 695417.
9. Arciola, C. R.; Campoccia, D.; Montanaro, L. Implant infections: adhesion, biofilm formation and immune evasion. *Nat Rev Microbiol.* **2018**, *16*, 397-409.
10. Kim, K. T.; Eo, M. Y.; Nguyen, T. T. H.; Kim, S. M. General review of titanium toxicity. *Int J Implant Dent.* **2019**, *5*, 10.
11. Gittens, R. A.; Olivares-Navarrete, R.; Schwartz, Z.; Boyan, B. D. Implant osseointegration and the role of microroughness and nanostructures: lessons for spine implants. *Acta Biomater.* **2014**, *10*, 3363-3371.
12. Schwarz, F.; Wieland, M.; Schwartz, Z.; Zhao, G.; Rupp, F.; Geis-Gerstorfer, J.; Schedle, A.; Broggini, N.; Bornstein, M. M.; Buser, D.; Ferguson, S. J.; Becker, J.; Boyan, B. D.; Cochran, D. L. Potential of chemically modified hydrophilic surface characteristics to support tissue integration of titanium dental implants. *J Biomed Mater Res B Appl Biomater.* **2009**, *88*, 544-557.
13. Kam, K. R.; Walsh, L. A.; Bock, S. M.; Ollerenshaw, J. D.; Ross, R. F.; Desai, T. A. The effect of nanotopography on modulating protein adsorption and the fibrotic response. *Tissue Eng Part A.* **2014**, *20*, 130-138.
14. Kaur, G.; Valarmathi, M. T.; Potts, J. D.; Jabbari, E.; Sabo-Attwood, T.; Wang, Q. Regulation of osteogenic differentiation of rat bone marrow stromal cells on 2D nanorod substrates. *Biomaterials.* **2010**, *31*, 1732-1741.
15. Kaur, G.; Valarmathi, M. T.; Potts, J. D.; Wang, Q. The promotion of osteoblastic differentiation of rat bone marrow stromal cells by a polyvalent plant mosaic virus. *Biomaterials.* **2008**, *29*, 4074-4081.
16. Kaur, G.; Wang, C.; Sun, J.; Wang, Q. The synergistic effects of multivalent ligand display and nanotopography on osteogenic differentiation of rat bone marrow stem cells. *Biomaterials.* **2010**, *31*, 5813-5824.
17. Lin, Y.; Su, Z.; Niu, Z.; Li, S.; Kaur, G.; Lee, L. A.; Wang, Q. Layer-by-layer assembly of viral capsid for cell adhesion. *Acta Biomater.* **2008**, *4*, 838-843.
18. Sitasuwan, P.; Lee, L. A.; Li, K.; Nguyen, H. G.; Wang, Q. RGD-conjugated rod-like viral nanoparticles on 2D scaffold improve bone differentiation of mesenchymal stem cells. *Front Chem.* **2014**, *2*, 31.
19. Metavarayuth, K.; Maturavongsadit, P.; Chen, X.; Sitasuwan, P.; Lu, L.; Su, J.; Wang, Q. Nanotopographical cues mediate osteogenesis of stem cells on virus substrates through BMP-2 intermediate. *Nano Lett.* **2019**, *19*, 8372-8380.
20. Metavarayuth, K.; Villarreal, E.; Wang, H.; Wang, Q. Surface

topography and free energy regulate osteogenesis of stem cells: effects of shape-controlled gold nanoparticles. *Biomater Transl.* **2021**, *2*, 165-173.

21. Robin, A.; Bernardes de Almeida Ribeiro, M.; Luiz Rosa, J.; Zenhei Nakazato, R.; Borges Silva, M. Formation of TiO_2 nanotube layer by anodization of titanium in ethylene Glycol-H_2O electrolyte. *J Surf Eng Mater Adv Technol.* **2014**, *4*, 123-130.
22. Brammer, K. S.; Frandsen, C. J.; Jin, S. TiO_2 nanotubes for bone regeneration. *Trends Biotechnol.* **2012**, *30*, 315-322.
23. Kulkarni, M.; Mazare, A.; Gongadze, E.; Perutkova, Š.; Kralj-Iglič, V.; Milošev, I.; Schmuki, P.; Iglič, A.; Mozetič, M. Titanium nanostructures for biomedical applications. *Nanotechnology.* **2015**, *26*, 062002.
24. Strnad, G.; Petrovan, C.; Russu, O.; Jakab-Farkas, L. TiO_2 nanostructured surfaces for biomedical applications developed by electrochemical anodization. *IOP Conference Series: Materials Science and Engineering.* **2016**, *161*, 012051.
25. Dalby, M. J.; Gadegaard, N.; Oreffo, R. O. Harnessing nanotopography and integrin-matrix interactions to influence stem cell fate. *Nat Mater.* **2014**, *13*, 558-569.
26. Wang, N.; Butler, J. P.; Ingber, D. E. Mechanotransduction across the cell surface and through the cytoskeleton. *Science.* **1993**, *260*, 1124-1127.
27. Ravichandran, R.; Liao, S.; Ng, C.; Chan, C. K.; Raghunath, M.; Ramakrishna, S. Effects of nanotopography on stem cell phenotypes. *World J Stem Cells.* **2009**, *1*, 55-66.
28. Oh, S.; Brammer, K. S.; Li, Y. S.; Teng, D.; Engler, A. J.; Chien, S.; Jin, S. Stem cell fate dictated solely by altered nanotube dimension. *Proc Natl Acad Sci U S A.* **2009**, *106*, 2130-2135.
29. Park, J. H.; Gu, L.; von Maltzahn, G.; Ruoslahti, E.; Bhatia, S. N.; Sailor, M. J. Biodegradable luminescent porous silicon nanoparticles for *in vivo* applications. *Nat Mater.* **2009**, *8*, 331-336.
30. Park, J.; Bauer, S.; Schmuki, P.; von der Mark, K. Narrow window in nanoscale dependent activation of endothelial cell growth and differentiation on TiO_2 nanotube surfaces. *Nano Lett.* **2009**, *9*, 3157-3164.
31. Yu, W. Q.; Jiang, X. Q.; Zhang, F. Q.; Xu, L. The effect of anatase TiO_2 nanotube layers on MC3T3-E1 preosteoblast adhesion, proliferation, and differentiation. *J Biomed Mater Res A.* **2010**, *94*, 1012-1022.
32. Zhao, L.; Liu, L.; Wu, Z.; Zhang, Y.; Chu, P. K. Effects of micropitted/nanotubular titania topographies on bone mesenchymal stem cell osteogenic differentiation. *Biomaterials.* **2012**, *33*, 2629-2641.
33. Lai, M.; Cai, K.; Zhao, L.; Chen, X.; Hou, Y.; Yang, Z. Surface functionalization of TiO2 nanotubes with bone morphogenetic protein 2 and its synergistic effect on the differentiation of mesenchymal stem cells. *Biomacromolecules.* **2011**, *12*, 1097-1105.
34. Smith, B. S.; Yoriya, S.; Johnson, T.; Popat, K. C. Dermal fibroblast and epidermal keratinocyte functionality on titania nanotube arrays. *Acta Biomater.* **2011**, *7*, 2686-2696.
35. Zhang, Y.; Luo, R.; Tan, J.; Wang, J.; Lu, X.; Qu, S.; Weng, J.; Feng, B. Osteoblast behaviors on titania nanotube and mesopore layers. *Regen Biomater.* **2017**, *4*, 81-87.
36. Park, J.; Bauer, S.; von der Mark, K.; Schmuki, P. Nanosize and vitality: TiO_2 nanotube diameter directs cell fate. *Nano Lett.* **2007**, *7*, 1686-1691.
37. Boussu, K.; Van der Bruggen, B.; Volodin, A.; Snauwaert, J.; Van Haesendonck, C.; Vandecasteele, C. Roughness and hydrophobicity studies of nanofiltration membranes using different modes of AFM. *J Colloid Interface Sci.* **2005**, *286*, 632-638.
38. Lee, L. A.; Nguyen, Q. L.; Wu, L.; Horvath, G.; Nelson, R. S.; Wang, Q. Mutant plant viruses with cell binding motifs provide differential adhesion strengths and morphologies. *Biomacromolecules.* **2012**, *13*, 422-431.
39. Nadri, S.; Soleimani, M. Comparative analysis of mesenchymal stromal cells from murine bone marrow and amniotic fluid. *Cytotherapy.* **2007**, *9*, 729-737.
40. Ito, H.; Uchida, T.; Makita, K. Interactions between rat alveolar epithelial cells and bone marrow-derived mesenchymal stem cells: an *in vitro* co-culture model. *Intensive Care Med Exp.* **2015**, *3*, 53.
41. Schneider, C. A.; Rasband, W. S.; Eliceiri, K. W. NIH Image to ImageJ: 25 years of image analysis. *Nat Methods.* **2012**, *9*, 671-675.
42. Doube, M.; Kłosowski, M. M.; Arganda-Carreras, I.; Cordelières, F. P.; Dougherty, R. P.; Jackson, J. S.; Schmid, B.; Hutchinson, J. R.; Shefelbine, S. J. BoneJ: free and extensible bone image analysis in ImageJ. *Bone.* **2010**, *47*, 1076-1079.
43. Guan, D.; Wang, Y. Synthesis and growth mechanism of multilayer TiO_2 nanotube arrays. *Nanoscale.* **2012**, *4*, 2968-2977.
44. Regonini, D.; Bowen, C. R.; Jaroenworaluck, A.; Stevens, R. A review of growth mechanism, structure and crystallinity of anodized TiO2 nanotubes. *Mater Sci Eng R Rep.* **2013**, *74*, 377-406.
45. Brammer, K. S.; Oh, S.; Frandsen, C. J.; Jin, S. Biomaterials and biotechnology schemes utilizing TiO_2 nanotube arrays. In Biomaterials science and engineering, IntechOpen: London, United Kingdom, 2011.
46. Zamudio Torres, I.; Pérez Bueno, J. J.; Meas Vong, Y. Process of growth TiO_2 nanotubes by anodization in an organic media. In Microscopy: advances in scientific research and education, Méndez-Vilas, A., Ed. Formatex: **2014**; pp 887-893.
47. Ozkan, S.; Nguyen, N. T.; Mazare, A.; Cerri, I.; Schmuki, P. Controlled spacing of self-organized anodic TiO_2 nanotubes. *Electrochem Commun.* **2016**, *69*, 76-79.
48. Yoriya, S.; Mor, G. K.; Sharma, S.; Grimes, C. A. Synthesis of ordered arrays of discrete, partially crystalline titania nanotubes by Ti anodization using diethylene glycol electrolytes. *J Mater Chem.* **2008**, *18*, 3332-3336.
49. Valota, A.; LeClere, D. J.; Skeldon, P.; Curioni, M.; Hashimoto, T.; Berger, S.; Kunze, J.; Schmuki, P.; Thompson, G. E. Influence of water content on nanotubular anodic titania formed in fluoride/glycerol electrolytes. *Electrochim Acta.* **2009**, *54*, 4321-4327.
50. Ferraris, S.; Spriano, S.; Pan, G.; Venturello, A.; Bianchi, C. L.; Chiesa, R.; Faga, M. G.; Maina, G.; Vernè, E. Surface modification of Ti-6Al-4V alloy for biomineralization and specific biological response: Part I, inorganic modification. *J Mater Sci Mater Med.* **2011**, *22*, 533-545.
51. Albu, S. P.; Roy, P.; Virtanen, S.; Schmuki, P. Self-organized TiO_2 nanotube arrays: critical effects on morphology and growth. *Isr J Chem.* **2010**, *50*, 453-467.
52. Bauer, S.; Kleber, S.; Schmuki, P. TiO_2 nanotubes: Tailoring the geometry in H_3PO_4/HF electrolytes. *Electrochem Commun.* **2006**, *8*, 1321-1325.
53. Yin, H.; Liu, H.; Shen, W. Z. The large diameter and fast growth of self-organized TiO_2 nanotube arrays achieved via electrochemical anodization. *Nanotechnology.* **2010**, *21*, 035601.
54. Bauer, S.; Park, J.; Faltenbacher, J.; Berger, S.; von der Mark, K.; Schmuki, P. Size selective behavior of mesenchymal stem cells on ZrO(2) and TiO(2) nanotube arrays. *Integr Biol (Camb).* **2009**, *1*, 525-532.
55. Sánchez-Tovar, R.; Lee, K.; García-Antón, J.; Schmuki, P. Formation of anodic TiO_2 nanotube or nanosponge morphology determined by the electrolyte hydrodynamic conditions. *Electrochem Commun.* **2013**, *26*, 1-4.
56. Law, K. Y. Definitions for hydrophilicity, hydrophobicity, and superhydrophobicity: getting the basics right. *J Phys Chem Lett.* **2014**, *5*,

686-688.
57. Lamour, G.; Hamraoui, A.; Buvailo, A.; Xing, Y.; Keuleyan, S.; Prakash, V.; Eftekhari-Bafrooei, A.; Borguet, E. Contact angle measurements using a simplified experimental setup. *J Chem Educ.* **2010**, *87*, 1403-1407.
58. Liu, G.; Du, K.; Wang, K. Surface wettability of TiO_2 nanotube arrays prepared by electrochemical anodization. *Appl Surf Sci.* **2016**, *388*, 313-320.
59. Ozcan, M.; Allahbeickaraghi, A.; Dündar, M. Possible hazardous effects of hydrofluoric acid and recommendations for treatment approach: a review. *Clin Oral Investig.* **2012**, *16*, 15-23.
60. Everett, E. T. Fluoride's effects on the formation of teeth and bones, and the influence of genetics. *J Dent Res.* **2011**, *90*, 552-560.
61. Zareidoost, A.; Yousefpour, M.; Ghaseme, B.; Amanzadeh, A. The relationship of surface roughness and cell response of chemical surface modification of titanium. *J Mater Sci Mater Med.* **2012**, *23*, 1479-1488.
62. Metavarayuth, K.; Sitasuwan, P.; Zhao, X.; Lin, Y.; Wang, Q. Influence of surface topographical cues on the differentiation of mesenchymal stem cells *in vitro*. *ACS Biomater Sci Eng.* **2016**, *2*, 142-151.
63. Gstraunthaler, G.; Lindl, T.; van der Valk, J. A plea to reduce or replace fetal bovine serum in cell culture media. *Cytotechnology.* **2013**, *65*, 791-793.
64. Heger, J. I.; Froehlich, K.; Pastuschek, J.; Schmidt, A.; Baer, C.; Mrowka, R.; Backsch, C.; Schleußner, E.; Markert, U. R.; Schmidt, A. Human serum alters cell culture behavior and improves spheroid formation in comparison to fetal bovine serum. *Exp Cell Res.* **2018**, *365*, 57-65.
65. Fang, C. Y.; Wu, C. C.; Fang, C. L.; Chen, W. Y.; Chen, C. L. Long-term growth comparison studies of FBS and FBS alternatives in six head and neck cell lines. *PLoS One.* **2017**, *12*, e0178960.
66. Bratengeier, C. *Mechanisms of mechanically induced Osteoclastogenesis : in a novel in vitro model for bone implant loosening*. Linköping University: Norrköping. **2019**.
67. Li, P. P.; Gu, C.; Liang, B. Y.; Wang, L.; Zhou, Y.; Tan, W. S. A serum-free medium suitable for maintaining cell morphology and liver-specific function in induced human hepatocytes. *Cytotechnology.* **2019**, *71*, 329-344.
68. Khalili, A. A.; Ahmad, M. R. A review of cell adhesion studies for biomedical and biological applications. *Int J Mol Sci.* **2015**, *16*, 18149-18184.
69. Chen, S.; Guo, Y.; Liu, R.; Wu, S.; Fang, J.; Huang, B.; Li, Z.; Chen, Z.; Chen, Z. Tuning surface properties of bone biomaterials to manipulate osteoblastic cell adhesion and the signaling pathways for the enhancement of early osseointegration. *Colloids Surf B Biointerfaces.* **2018**, *164*, 58-69.
70. Xi, A.; Bothun, G. D. Centrifugation-based assay for examining nanoparticle-lipid membrane binding and disruption. *Analyst.* **2014**, *139*, 973-981.
71. Franco-Barraza, J.; Beacham, D. A.; Amatangelo, M. D.; Cukierman, E. Preparation of extracellular matrices produced by cultured and primary fibroblasts. *Curr Protoc Cell Biol.* **2016**, *71*, 10.19.11-10.19.34.
72. Khan, R. S.; Newsome, P. N. A comparison of phenotypic and functional properties of mesenchymal stromal cells and multipotent adult progenitor cells. *Front Immunol.* **2019**, *10*, 1952.
73. Hong, S. H.; Lee, M. H.; Koo, M. A.; Seon, G. M.; Park, Y. J.; Kim, D.; Park, J. C. Stem cell passage affects directional migration of stem cells in electrotaxis. *Stem Cell Res.* **2019**, *38*, 101475.
74. Zheng, H.; Martin, J. A.; Duwayri, Y.; Falcon, G.; Buckwalter, J. A. Impact of aging on rat bone marrow-derived stem cell chondrogenesis. *J Gerontol A Biol Sci Med Sci.* **2007**, *62*, 136-148.
75. Higuchi, A.; Shimmura, S.; Takeuchi, T.; Suematsu, M.; Tsubota, K. Elucidation of apoptosis induced by serum deprivation in cultured conjunctival epithelial cells. *Br J Ophthalmol.* **2006**, *90*, 760-764.
76. Alberts, B.; Johnson, A.; Lewis, J.; Raff, M.; Roberts, K.; Walter, P. Molecular biology of the cell. 4th ed. Garland Science: New York,**2002**.
77. Schwartz, M. A. Integrins and extracellular matrix in mechanotransduction. *Cold Spring Harb Perspect Biol.* **2010**, *2*, a005066.
78. Wozniak, M. A.; Modzelewska, K.; Kwong, L.; Keely, P. J. Focal adhesion regulation of cell behavior. *Biochim Biophys Acta.* **2004**, *1692*, 103-119.
79. Mirbagheri, M.; Adibnia, V.; Hughes, B. R.; Waldman, S. D.; Banquy, X.; Hwang, D. K. Advanced cell culture platforms: a growing quest for emulating natural tissues. *Mater Horiz.* **2019**, *6*, 45-71.
80. Arnold, M.; Cavalcanti-Adam, E. A.; Glass, R.; Blümmel, J.; Eck, W.; Kantlehner, M.; Kessler, H.; Spatz, J. P. Activation of integrin function by nanopatterned adhesive interfaces. *Chemphyschem.* **2004**, *5*, 383-388.
81. Kim, D. H.; Provenzano, P. P.; Smith, C. L.; Levchenko, A. Matrix nanotopography as a regulator of cell function. *J Cell Biol.* **2012**, *197*, 351-360.
82. Reyes, C. D.; Petrie, T. A.; Burns, K. L.; Schwartz, Z.; García, A. J. Biomolecular surface coating to enhance orthopaedic tissue healing and integration. *Biomaterials.* **2007**, *28*, 3228-3235.
83. Wojtowicz, A. M.; Shekaran, A.; Oest, M. E.; Dupont, K. M.; Templeman, K. L.; Hutmacher, D. W.; Guldberg, R. E.; García, A. J. Coating of biomaterial scaffolds with the collagen-mimetic peptide GFOGER for bone defect repair. *Biomaterials.* **2010**, *31*, 2574-2582.
84. Hanawa, T. Titanium-tissue interface reaction and its control with surface treatment. *Front Bioeng Biotechnol.* **2019**, *7*, 170.
85. Tapscott, D. C.; Wottowa, C. Orthopedic implant materials. In StatPearls, StatPearls Publishing: Treasure Island (FL), **2022**.
86. Wang, W.; Poh, C. K. Titanium alloys in orthopaedics. In *Titanium alloys - advances in properties control*, Sieniawski, J.; Ziaja, W., eds.; IntechOpen: London, **2013**.
87. Kim, Y. H.; Choi, M.; Kim, J. W. Are titanium implants actually safe for magnetic resonance imaging examinations? *Arch Plast Surg.* **2019**, *46*, 96-97.
88. Mendonça, G.; Mendonça, D. B.; Aragão, F. J.; Cooper, L. F. Advancing dental implant surface technology--from micron- to nanotopography. *Biomaterials.* **2008**, *29*, 3822-3835.
89. Pachauri, P.; Bathala, L. R.; Sangur, R. Techniques for dental implant nanosurface modifications. *J Adv Prosthodont.* **2014**, *6*, 498-504.
90. Bressan, E.; Sbricoli, L.; Guazzo, R.; Tocco, I.; Roman, M.; Vindigni, V.; Stellini, E.; Gardin, C.; Ferroni, L.; Sivolella, S.; Zavan, B. Nanostructured surfaces of dental implants. *Int J Mol Sci.* **2013**, *14*, 1918-1931.
91. Baena, R. R. y.; Rizzo, S.; Manzo, L.; Lupi, S. M.; Andersson, M. Nanofeatured titanium surfaces for dental implantology: biological effects, biocompatibility, and safety. *J Nanomaterials.* **2017**, *2017*, 18.
92. Roy, P.; Berger, S.; Schmuki, P. TiO_2 nanotubes: synthesis and applications. Angew *Chem Int Ed Engl.* **2011**, *50*, 2904-2939.
93. Lee, W.; Scholz, R.; Gösele, U. A continuous process for structurally well-defined Al_2O_3 nanotubes based on pulse anodization of aluminum. *Nano Lett.* **2008**, *8*, 2155-2160.
94. Minagar, S.; Berndt, C. C.; Wang, J.; Ivanova, E.; Wen, C. A review of the application of anodization for the fabrication of nanotubes on metal implant surfaces. *Acta Biomater.* **2012**, *8*, 2875-2888.
95. Mohan, L.; Kar, S.; Nandhini, B.; Kumar, S. S. D.; Nagai, M.; Santra,

T. S. Formation of nanostructures on magnesium alloy by anodization for potential biomedical applications. *Mater Today Commun.* **2020**, *25*, 101403.

96. Rani, R. A.; Zoolfakar, A. S.; Ou, J. Z.; Kadir, R. A.; Nili, H.; Latham, K.; Sriram, S.; Bhaskaran, M.; Zhuiykov, S.; Kaner, R. B.; Kalantar-zadeh, K. Reduced impurity-driven defect states in anodized nanoporous Nb_2O_5: the possibility of improving performance of photoanodes. *Chem Commun (Camb).* **2013**, *49*, 6349-6351.
97. Dobosz, I. Influence of the anodization conditions and chemical treatment on the formation of alumina membranes with defined pore diameters. *J Porous Mater.* **2021**, *28*, 1011-1022.
98. Quinn, J.; McFadden, R.; Chan, C. W.; Carson, L. Titanium for orthopedic applications: an overview of surface modification to improve biocompatibility and prevent bacterial biofilm formation. *iScience.* **2020**, *23*, 101745.
99. Mansoorianfar, M.; Tavoosi, M.; Mozafarinia, R.; Ghasemi, A.; Doostmohammadi, A. Preparation and characterization of TiO2 nanotube arrays on Ti6Al4V surface for enhancement of cell treatment. *Surf Coat Technol.* **2017**, *321*, 409-415.
100. Popat, K. C.; Leoni, L.; Grimes, C. A.; Desai, T. A. Influence of engineered titania nanotubular surfaces on bone cells. *Biomaterials.* **2007**, *28*, 3188-3197.
101. Li, Y.; Li, B.; Fu, X.; Li, J.; Li, C.; Li, H.; Li, H.; Liang, C.; Wang, H.; Zhou, L.; Xin, S. Anodic oxidation modification improve bioactivity and biocompatibility of titanium implant surface. *J Hard Tissue Biol.* **2013**, *22*, 351-358.

Received: August 26, 2022
Revised: September 7, 2022
Accepted: September 17, 2022
Available online: September 28, 2022